

GaitFormer: Revisiting Intrinsic Periodicity for Gait Recognition

Qian Wu
MEGVII Technology
wuqian@megvii.com

Ruixuan Xiao*
Zhejiang University
xiaoruixuan@zju.edu.cn

Kaixin Xu*
Fudan University
kxxu22@m.fudan.edu.cn

Jingcheng Ni*
Behang University
kiranjc@buaa.edu.cn

Boxun Li
MEGVII Technology
liboxun@megvii.com

Ziyao Xu
MEGVII Technology
xuziyao@megvii.com

Abstract

Gait recognition aims to distinguish different walking patterns by analyzing video-level human silhouettes, rather than relying on appearance information. Previous research on gait recognition has primarily focused on extracting local or global spatial-temporal representations, while overlooking the intrinsic periodic features of gait sequences, which, when fully utilized, can significantly enhance performance. In this work, we propose a plug-and-play strategy, called Temporal Periodic Alignment (TPA), which leverages the periodic nature and fine-grained temporal dependencies of gait patterns. The TPA strategy comprises two key components. The first component is Adaptive Fourier-transform Position Encoding (AFPE), which adaptively converts features and discrete-time signals into embeddings that are sensitive to periodic walking patterns. The second component is the Temporal Aggregation Module (TAM), which separates embeddings into trend and seasonal components, and extracts meaningful temporal correlations to identify primary components, while filtering out random noise. We present a simple and effective baseline method for gait recognition, based on the TPA strategy. Extensive experiments conducted on three popular public datasets (CASIA-B, OU-MVLP, and GREW) demonstrate that our proposed method achieves state-of-the-art performance on multiple benchmark tests.

1. Introduction

Biometrics technology aims to identify different people with various physiological characteristics, such as faces, fingerprints, iris, and DNA. Compared with other biometrics, human gait, the walking pattern of an individual, could be easily obtained at a distance without the cooperation of

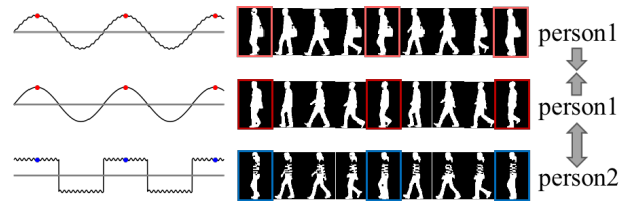


Figure 1: Based on our observations and statistical analysis, gait sequences exhibit distinct periods that are consistent across most individuals in the CASIA-B dataset. The accompanying waveform illustrates that each gait sequence is composed of several similar periods containing approximately 30 frames. The silhouettes sampled from CASIA-B, arranged from top to bottom, provide a visual representation of these periods.

interest-subjects. Moreover, it is difficult to camouflage, making it promising for forensic identification, crime prevention, and suspect tracing.

However, human gaits are usually captured in complex conditions, including cross-view, pose, carrying, clothing, aging, illumination and occlusions, which have posed a ubiquitous obstacle [6, 27, 51, 40, 37]. Thus the core challenge of gait recognition lies in learning discriminative and invariant spatial-temporal features under such unconstrained conditions. From the perspective of temporal information learning, existing approaches can be roughly divided into three types: template-based, image-based, and sequence-based approaches. Template-based approaches directly employ the DNN on single gait templates to extract discriminative representations [41, 52]. Image-based methods process frames independently with each other, then fuse temporal features with simple operations [3, 13, 29]. The aforementioned methods rarely take into account the global and local interaction of temporal features. On the contrary, sequence-based approaches regard sequences as videos and apply LSTM [16], 3D-CNN or Set Transformer [22] to fuse

*Work done during the internship at MEGVII Technology.

every frame for comprehensive motion investigation [14]. Despite the success, the sequence-based approaches simply apply temporal modules to process the sequence-level information, but rarely employ adaptation to cope with the intrinsic periodicity of gait sequences. At that point, the natural periodic inductive bias gets overlooked, which retains great potential for boosted performance.

As a periodic motion, each gait sequence can be regarded as the combination of several analogous walking periods, as shown in Figure 1. Based on the observations of different gait periods, fine-grained similarities and differences inside the same period, as well as phase alignment problems caused by multi-view sequences, we believe that it is a difficult and important task to adaptively encode the temporal periodic relationship. To better exploit such periodic nature, we propose a plug-in module termed Temporal Periodic Alignment (TPA) in this paper. Key to our methods, TPA enhances the capacity of the transformer modules in exploiting temporal periodicity with two components, the first one is the Adaptive Fourier-transform Position Encoding (AFPE) which injects the periodic prior with adaptively superimposed position encodings based on Fourier-transform to generate the discriminative period-aware embeddings. Second, the period-aware embeddings are fed forward into the Temporal Aggregation Module (TAM) with explicit feature frequency decomposition and aggregation to explore the fine-grained dependencies.

Empirically, existing sequence-based baselines exhibit a performance enhancement when equipped with TPA strategy. We take a further step and establish a simple yet strong baseline named GaitFormer. We conduct extensive experiments on different benchmarks to demonstrate the effectiveness of our proposed method. In summary, our contributions are as follows:

- We propose Adaptive Fourier-transform Position Encoding (AFPE) module to force periodic prior for gait recognition. To the best of our knowledge, this is the first work to take full advantage of temporal periodicity.
- We present a plug-and-play strategy named Temporal Periodic Alignment (TPA), consisting of the novel AFPE and Temporal Aggregation Module (TAM). We further build a simple yet strong baseline GaitFormer based on the TPA module.
- By providing comprehensive experimental results, we show that the TPA module boosts the performance of existing methods as a plug-in complement. Moreover, our new proposed baseline GaitFormer outperforms SOTA methods on OU-MVLP (91.6%), CASIA-B (98.9%, normal) and GREW (64.8%) datasets.

2. Related Work

Gait Recognition. Recent works for gait recognition can be mainly categorized into three types: template-based, image-based, and sequence-based approaches.

Early template-based methods directly employ the DNN on single gait templates to extract discriminate representations [41, 52, 28]. Gait Energy Image (GEI) [15] is proposed as the temporal compression of a silhouette sequence for following template matching. Different architectures for CNNs are integrated [49] to facilitate cross-view gait recognition. Despite the simplicity of the template-based method, temporal and partial information might be missing during the template compression and the extracted representations tend to be sensitive to occlusion changes.

For the image-based strand [25, 2], GaitSet [3] incorporates horizontal segmentation and pyramid mapping to extract multi-scale spatial representations and aggregate them into a set-level feature. GaitPart [13] adopts the Focal Convolution Layer to enhance the part-level spatial features. GLN [18] leveraged the inherent feature pyramid to obtain more abundant spatial information. However, these methods neglect the motion changes and lost the dependencies of each part at different times during walking.

The sequence-based approaches [10, 26] regard the silhouettes of a gait sequence as a video for the comprehensive investigation of motion. Early methods [14, 35] adopt LSTM to extract the temporal relationship within segmented partitions.

Xing et al. [50], Zhen et al. [20] and GaitGL [29] proposed 3D-CNN to capture spatial and temporal information simultaneously. TransGait [23] proposed Set Transformer to fuse sequence information while regarding gait sequences as sets. MetaGait [11] learns omni-sample adaptive representation on spatial, temporal and channel dimensions. Despite the success, these methods mostly integrate temporal representations with relatively simple paradigms and underemphasize the periodic inductive bias of gait recognition, whose capability is severely underestimated. In this paper, we advocate a temporal periodic alignment strategy to learn the periodic prior.

Periodicity in Gait Analysis. Cunado et al. [7] applied Fourier Transform on two angle sequences from legs of model-based gait sequences to extract temporal features. An et al. [1] utilized temporal normalize to sample a complete period from the gait sequences, which is different from our random sampling strategy to adaptively learn the periodic information. Li et al. [24] exploit phase estimation method to explicitly synchronize the gait sequences under different views. On the contrary, we implicitly encode the sequences of different phases through AFPE to obtain phase-agnostic information extraction.

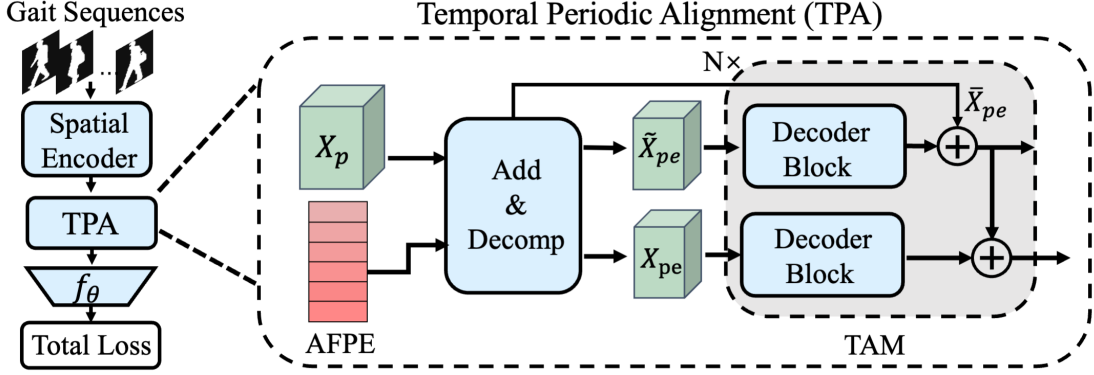


Figure 2: Overview of the whole framework of our proposed GaitFormer. The Spatial Encoder generates the spatial feature X_p . Next, the AFPE encodes the discrete-time signals, added with X_p , generating period-aware embedding. Then, the embedding is decomposed into trend \tilde{X}_{pe} and seasonal part \bar{X}_{pe} . They are sent to N TAM blocks to learn temporal correlation information. Finally, a header f_θ , consisting of BN and linear perception, is applied to map the feature vectors to the classification and metric space. Only the feature for metric learning is retained in the test stage.

Transformer and Positional Encoding. Transformer [46] has achieved remarkable achievements in natural language processing and computer vision. Vision Transformer [9] and its variants [31, 32] have shown to excel and led to remarkable progress in visual recognition. Given the advantages in capturing correlations within long sequences, it is reasonable to apply this architecture to gait recognition.

Positional encoding encrypts the positional correlation of the input sequence, which is crucial in Transformer-based long-sequence learning. Besides the vanilla positional encoding, several meticulously designed variants have recently been proposed [4, 30] for different tasks.

In this paper, based on the periodicity of gait recognition, we make the first attempt to apply the Fourier-transform to generate a series of base sequences and adaptively aggregate them as positional encoding, simulating periodic posture changes of pedestrians walking.

3. Method

In this section, we first define the formulation and outline the framework of our method. Then we elaborate on the temporal periodic alignment (TPA) strategy, which encapsulates the Adaptive Fourier-transform Position Encoding (AFPE) and Temporal Aggregation Module (TAM). Finally, we describe the details of the GaitFormer which is a simple yet strong baseline established on the basis of TPA.

3.1. Architecture Overview

The overview of our proposed pipeline is shown in Figure 2. The Spatial Encoder comprises a CNN backbone and HP module, which is a common setting in GaitPart and OpenGait [12]. For a gait sequence from source dataset, the input frames are sampled as $X_i \in \mathbb{R}^{C_i \times T_i \times H_i \times W_i}$, where

C_i denotes the channel number of the silhouette, T_i is the length of the sampled sequence and (H_i, W_i) represents the image shape. The backbone generates output feature maps as $X_o \in \mathbb{R}^{C_o \times T_o \times H_o \times W_o}$, where C_o is output channel of the backbone. Since no downsampling occurs in the temporal dimension, T_o is same as T_i , while the spatial shape of silhouettes undergoes downsampling twice. Next, the Horizontal Pooling (HP) [3] module is applied to extract discriminative part-informed features $X_p \in \mathbb{R}^{P \times C_o \times T_o}$, where P represents the number of horizontally split parts.

Then, the part-level features are sent into TPA strategy. Specifically, the features are firstly fused with AFPE, followed by several blocks of TAM to learn the temporal correlation information within each sequence. Therefore, the output feature of TPA is denoted as $X_t \in \mathbb{R}^{P \times C_t}$, where C_t is the channel of the output.

Finally, we use several separate BN [21] and linear perception layers, represented as f_θ , to map the feature vectors to the classification and metric space for gait recognition.

3.2. Temporal Periodic Alignment

As aforementioned, previous works on gait recognition mostly focus on extracting better spatial representations, while underemphasizing the periodic dependencies along the temporal dimension. To overcome this weakness, we present a plug-and-play strategy termed Temporal Periodic Alignment (TPA) to force the periodic prior and explore fine-grained temporal dependencies, which comprise two key components AFPE and TAM in what follows.

3.2.1 Adaptive Fourier-transform Position Encoding

In order to better exploit the temporal correlation within the long gait sequence, we resort to the transformer network

and design our TPA module based on the attention mechanism. Position encoding (PE) encodes the relative positional relationship in the transformer blocks. Considering that vanilla position encoding (PE) regards each element in the sequence as unique and thus fails to capture the periodic correlation variations, we aim to inject the periodic inductive bias in the position encoding. Based on the observations on differences in periods between different people, fine-grained similarity within period and phase align problems, we incorporate a Fourier transform to generate a series of base position encodings with different frequencies and rely on a position encoder to adaptively aggregate the final position encoding to represent ever-changing periodic information.

Specifically, the Discrete Fourier transform (DFT) is a mathematical transform that decomposes functions depending on space or time into its discrete frequencies, and the Inverse Discrete Fourier Transform (IDFT) is the inverse of DFT. According to Euler’s formula, $e^{-i\theta} = \cos(\theta) - i \cdot \sin(\theta)$, given an origin sequence $\{x_t\}$, containing T elements, and a set of base sequences $\{X_k\}$, where $k \in [0, T - 1]$, the IDFT is defined by the formula:

$$\begin{aligned} x_t &= \frac{1}{T} \sum_{k=1}^{T-1} X_k \cdot e^{i\frac{2\pi}{T}kt}, \quad t \in [0, T - 1] \\ &= \frac{1}{T} \sum_{k=1}^{T-1} X_k \cdot \left(\cos\left(\frac{2\pi}{T}kt\right) + i \cdot \sin\left(\frac{2\pi}{T}kt\right) \right) \end{aligned} \quad (1)$$

Inspired by the above principles, as well as the idea of PETR [30], in which the real physical location information in the image is transformed into the position encoding, we propose AFPE to encode a series of discrete-time signals into the position encoding and extend the original embeddings into period-aware ones.

Specifically, for a sequence of length T , we sample T_d base sequences evenly from all T components of IDFT tokens with interval $d = \lfloor \frac{T}{T_d} \rfloor$ to reduce computation and complexity. Consequently, the downsampled set of base sequences $\{\hat{X}_k\}, k = \{d, 2 \cdot d, \dots, T_d \cdot d\}$ can be formulated:

$$\{\hat{X}_k\} = \left\{ \cos\left(\frac{2\pi}{T}kt\right), \sin\left(\frac{2\pi}{T}kt\right) \right\}, t \in [0, T - 1] \quad (2)$$

Then, the position encoding procession can be formulated as follows:

$$AFPE = \psi(\text{Concat}(\{\hat{X}_k\})) \quad (3)$$

where $\text{Concat}(\cdot)$ means stack all the base sequences on the channel dimension, ψ is the position encoding function, consists of a 2-layer Multi-Layer Perceptron (MLP), and the output shape is $AFPE \in \mathbb{R}^{T_i \times C_o}$.

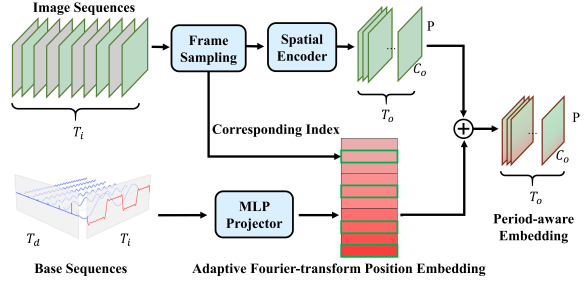


Figure 3: Illustration of the proposed Adaptive Fourier-transform Position Encoding (AFPE). The base sequences are sampled evenly from all DFT components. Then the bases are transformed into AFPE by a multi-layer perceptron. The corresponding index of the input frames is used to gather the relative AFPE. Finally, the AFPE is added with the features, producing period-aware embeddings.

Meanwhile, the indexes of the input frames are used to gather corresponding features from the AFPE, which aims at encoding the relative temporal correlation. The above-mentioned process can be expressed by the formula:

$$X_{pe} = X_p + \text{gather}(AFPE, \text{indexes}) \quad (4)$$

where X_p indicates the embedding feature of the HP module and X_{pe} is the period-aware embedding, indexes is the relative frame indexes of sampled input frames, $\text{gather}(\cdot)$ means sample the AFPE elements according to the indexes, as shown in Figure 3.

3.2.2 Temporal Aggregation Module

After embeddings of a sequence are injected with periodic prior through AFPE, the fine-grained temporal dependencies remain underexplored. In pursuit of grabbing features that are more related to the walking pattern and robust to view change, We revamp the vanilla decoder of transformer from the perspective of trend-seasonal decomposition.

Specifically, different from the traditional decoder module, the Decoder block of Temporal Periodic Module is composed of Multi-Head Cross-Attention (MHCA) [46] sub-layer and a position-wise fully connected feed-forward network (FFN), where the period-aware embeddings and class-tokens are directly sent into MHCA sub-layer to extract temporal information. In order to learn periodic temporal information, we decompose the inputting features into the trend-cyclical and the seasonal part, according to the common practice of time series forecasting problems [5]. Here, we set trend-cyclical as the average mean of a single gait period, which is about 30 frames according to statistical analysis. After that, origin features and seasonal features are sent to their respective transformer modules with corresponding tokens, then the output tokens are fused through

Methods	Probe View														Mean
	0°	15°	30°	45°	60°	75°	90°	180°	195°	210°	225°	240°	255°	270°	
GaitSet [3]	79.3	87.9	90.0	90.1	88.0	88.7	87.7	81.8	86.5	89.0	89.2	87.2	87.6	86.2	87.1
GaitPart [13]	82.6	88.9	90.8	91.0	89.7	89.9	89.5	85.2	88.1	90.0	90.1	89.0	89.1	88.2	88.7
GLN [18]	83.8	90.0	91.0	91.2	90.3	90.0	89.4	85.3	89.1	90.5	90.6	89.6	89.3	88.5	89.2
GaitGL [29]	84.9	90.2	91.1	91.5	91.1	90.8	90.3	88.5	88.6	90.3	90.4	89.6	89.5	88.8	89.7
ReverseMask [38]	87.9	91.5	91.7	92.0	92.0	91.6	91.3	90.7	90.3	90.9	91.1	90.8	90.5	90.2	90.9
3DLocal [20]	86.1	91.2	92.6	92.9	92.2	91.3	91.1	86.9	90.8	92.2	92.3	91.3	91.1	90.2	90.9
GaitFormer	89.6	92.3	92.1	92.4	92.5	91.9	91.7	91.5	91.6	91.5	91.7	91.7	91.2	91.0	91.6
GaitSet [3]	84.5	93.3	96.7	96.6	93.5	95.3	94.2	87.0	92.5	96.0	96.0	93.0	94.3	92.7	93.3
GaitPart [13]	88.0	94.7	97.7	97.6	95.5	96.6	96.2	90.6	94.2	97.2	97.1	95.1	96.0	95.0	95.1
GLN [18]	89.3	95.8	97.9	97.8	96.0	96.7	96.1	90.7	95.3	97.7	97.5	95.7	96.2	95.3	95.6
GaitGL [29]	90.5	96.1	98.0	98.1	97.0	97.6	97.1	94.2	94.9	97.4	97.4	95.7	96.5	95.7	96.2
ReverseMask [38]	93.7	97.5	98.6	98.8	98.0	98.5	98.2	96.5	96.7	98.2	98.1	97.1	97.6	97.2	97.5
GaitFormer	95.4	98.3	99.0	99.2	98.5	98.8	98.6	97.4	98.0	98.8	98.7	98.1	98.4	98.1	98.2

Table 1: Rank-1 accuracy (%) of the compared method on OU-MVLP under 14 probe views excluding identical-view cases. The top 7 rows and bottom 6 rows show the results with and without invalid probe sequences respectively.

linear lateral layers. TAM explicitly learns the frequency decomposition of features to balance temporal sensitivity and robustness. The procession can be described as follow:

$$\begin{aligned}
\hat{x}_{token}^i &= FFN(MHCA(x_{token}^{i-1}, X_{pe})) \\
\tilde{x}_{token}^i &= FFN(MHCA(\hat{x}_{token}^{i-1}, \tilde{X}_{pe})) \\
x_{token}^i &= Fusion(\hat{x}_{token}^i, Lateral(\bar{X}_{pe} + \tilde{x}_{token}^i))
\end{aligned} \tag{5}$$

where \bar{X}_{pe} and \tilde{X}_{pe} are the calculated trend-cyclical and seasonal part of the embedding, x_{token}^{i-1} and \hat{x}_{token}^i indicate the token for full feature of previous transformer block and current i th block. \hat{x}_{token}^i represents the token for residual fusion, while \tilde{x}_{token}^i indicates the token for seasonal feature. The $Lateral(\cdot)$ function can be one MLP layer, meanwhile the $Fusion(\cdot)$ function is $Mean(\cdot)$ in practice. Note that descriptions of operations like Layer-Norm and residual connection are omitted, which means they are the same as common practices.

3.3. Training objectives

In our work, we incorporate a combined loss, consist of triplet loss [17] and cross-entropy loss to effectively train the proposed gait recognition model. The temporal triplet loss aims to improve the inter-class distance and reduce the intra-class distance, which is more beneficial to distinguishing untrained human IDs. In our work, we adapt triplet loss with temporal dimension, to cope with the distance comparison between the temporal features.

$$L_{tri} = [Dist(\mathcal{F}(X_a), \mathcal{F}(X_p)) - Dist(\mathcal{F}(X_a), \mathcal{F}(X_n)) + m]_+ \tag{6}$$

where X_a and X_p are samples from the same class, X_n is from another class, \mathcal{F} represents our proposed feature ex-

tractor and mapping method. m is the margin of the triplet loss. The operation $[\cdot]_+$ is equal to $Max(\cdot, 0)$.

$$Dist(X, Y) = \frac{1}{T} \sum_{t=0}^{T-1} \sqrt{(x_t - y_t)^2} \tag{7}$$

Specifically, $Dist(\cdot)$ is the mean of Euclidean distances between x_t and y_t along temporal dimension.

Further, we replace the vanilla cross-entropy loss with ArcFace[8] loss to encourage a larger margin, which is denoted as L_{cls} . The combined loss L can be defined as:

$$L = p * L_{cls} + q * L_{tri} \tag{8}$$

where p and q are the weight of losses. The hyper-parameters in Equation 8 are described in Implementation Details.

4. Experiments

Our empirical experiments mainly consist of two parts. In the first part, extensive experiments are conducted on three popular gait datasets: CASIA-B [45], OU-MVLP [43] and GREW [53]. Then ablation experiments and analysis of the performance are given in the second part.

4.1. Datasets

CASIA-B dataset is the most popular gait dataset, including RGB images and silhouettes of 124 subjects with 10 sequences under 11 views (0°, 18°, ..., 180°). The 10 sequences contain 6 normal walking variants (NM), 2 variants with subjects carrying bags (BG), and 2 variants with subjects wearing different clothes (CL). Hence, each subject contains 10 (groups) × 11 (view angle) = 110 gait sequences. We strictly follow the popular protocol for evalu-

Methods	Rank-1	Rank-5	Rank-10	Rank-20
GEINet [42]	6.8	13.4	17.0	21.0
TS-CNN [48]	13.6	24.6	30.2	37.0
GaitSet [3]	46.3	63.6	70.3	76.8
GaitPart [13]	44.0	60.7	67.3	73.5
CSTL [19]	50.6	65.9	71.9	76.9
TransGait	56.27	72.72	78.12	82.51
GaitFormer	65.53	78.63	83.04	86.38

Table 2: Rank-1 accuracy (%), Rank-5 accuracy (%), Rank-10 accuracy (%), and Rank-20 accuracy (%) on the GREW dataset.

ation, which employs the first 74 subjects as the training set and the latter 50 subjects are reserved for testing.

OU-MVLP dataset is a larger public gait dataset created by Osaka University, which includes 10,307 subjects. Each subject was collected under 14 views between $[0^\circ, 90^\circ]$ and $[180^\circ, 270^\circ]$ with the interval of 15° , and each view consist of 2 video sequences (Seq#00 and Seq#01). During testing, the sequences in Seq#01 serve as the gallery set and those in Seq#00 are regarded as the probe set.

GREW dataset is the latest gait dataset which is more challenging. It consists of 26,345 subjects and 128,671 sequences, obtained with 882 cameras in wild environments. The GREW dataset has diverse and practical view variations, as well as more naturally challenging factors. Besides, the unconstrained setting also brings new challenging factors for gait patterns, such as diverse views, dressing, carrying, and crowd.

4.2. Implementaion Details

All models are implemented in PyTorch [36]. The silhouettes in both datasets are pre-processed using methods proposed in [44]. The input size is set to 64×44 . In a mini-batch, the number of subjects and the number of sequences are set to (8, 16) for CASIA-B and (32, 8) for OU-MVLP. In the training phase, we randomly sample the silhouettes from each gait sequence according to TSN sampling [47], the number of sampled frames is fixed at 30. While in the test phase, the silhouettes are sampled at the center of every segment.

AdamW [33] optimizer is used, while weight decay is set to $5e-1$. The learning rate is initialized to $1e-3$ and decreased to $1e-6$ in cosine decay style within 100,000 iterations. Besides, the warmup strategy is adopted at the start of training. As for hyperparameter settings in losses, the scale of Arcface loss s is set to 32 and the margin m is 0.3. Label smoothing is used to avoid overfitting. The margin thresh-

Methods	Probe			Mean
	NM	BG	CL	
GaitSet [3]	95.0	87.2	70.4	84.2
GaitPart [13]	96.2	91.5	78.7	88.8
ReverseMask [38]	97.7	95.3	86.0	93.0
GaitGL [29]	97.4	94.5	83.6	91.8
3DLocal [20]	97.5	94.3	83.7	91.8
GaitFormer	96.1	90.1	75.8	87.3
GaitSet+ [3]	96.9	92.6	81.7	90.4
GaitPart+ [13]	97.7	93.1	81.2	90.7
GaitGL+ [29]	98.5	95.3	85.8	93.2
GaitFormer+	98.9	94.7	87.3	93.6

Table 3: Rank-1 accuracy (%) of the compared method on CASIA-B under different conditions, excluding identical-view cases with the setting of large-scale training (LT). Here methods with '+' denote two-stage training, warm-up on OU-MVLP and continue the second stage of training and testing on CASIA-B dataset.

Methods	TPA	Mean Accuracy
GaitPart [13]	\times	88.7
	\checkmark	89.4
GaitGL [29]	\times	89.7
	\checkmark	90.4

Table 4: Results of baselines with and without TPA strategy on OU-MVLP dataset with invalid probe sequences.

old m for triplet loss is set to 0.2. The ratio of Equation 8 is set as $p = 0.1$ and $q = 1.0$.

The widely employed Rank-1 accuracy excluding identical-view sequences is taken as the evaluation metric for performance comparison. For the evaluation of CASIA-B, experiments are conducted with the setting LT.

4.3. Comparison with State-of-the-Art Methods

We first compare our method with several state-of-the-art methods including GaitSet [3], GaitPart [13], GaitGL [29], ReserveMask[39], TransGait [23], CSTL [19], TS-CNN [48] and 3DLocal [20] on the OU-MVLP, CASIA-B, and GREW datasets. The results are listed as follows.

4.3.1 Results on OU-MVLP

As shown in Table 1, GaitFormer outperforms all its counterparts and achieves new SOTA results under various cross-view conditions on the OU-MVLP dataset. Specifically, the average accuracy of our method achieves 91.6%, improved by 1.6% and 0.7% compared with advanced GaitGL and 3DLocal respectively. Besides, when the subjects in the

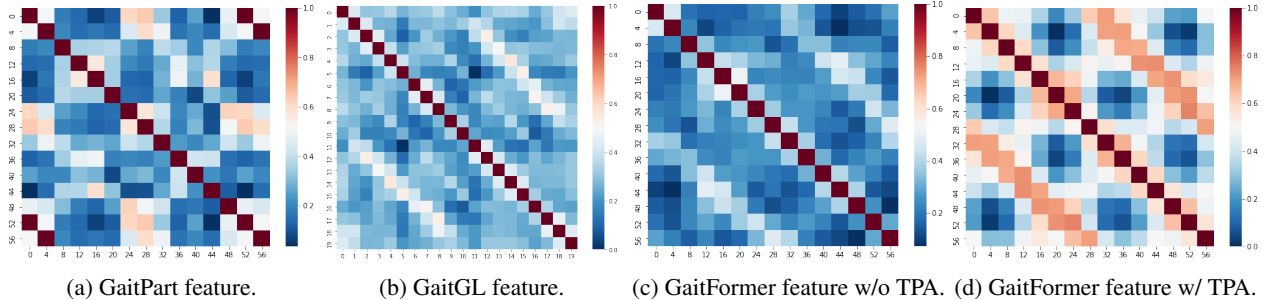


Figure 4: Visualization of self-similarity of temporal features in gait recognition models. (a) shows that except for itself, the similarity between the features 30 frames away is relatively high as well, indicating that GaitPart [13] with little temporal aggregation can learn the periodic information somehow. Similarity in (b) shows that GaitGL [29] learns better temporal periodic correlation. Correspondingly, (c) and (d) is the feature similarity of GaitFormer, with and without TPA respectively. It is obvious that the TPA module adaptively strengthens the periodic nature of temporal features. Note that, the horizontal and vertical coordinates in the heatmap represent frame indexes in the gait sequence, with red pixels indicating high similarity and blue the opposite. Due to 3D convolution with strides greater than 1, the frame number of (b) is less than others.

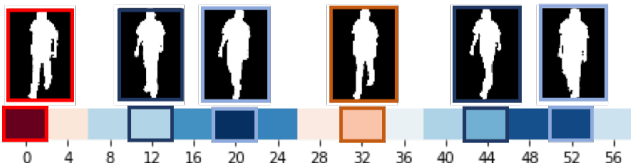


Figure 5: Visualization of silhouettes and feature similarity. The color bar is the first row of Figure 4d, in which red boxes mean high similarity and blue ones mean low. The silhouettes are sampled according to the corresponding indexes on the heatmap. We can observe that the silhouettes represented by features with higher similarity are more similar in appearance, and vice versa.

probe without corresponding samples are discarded, GaitFormer consistently leads by an even larger margin. The results demonstrate the superiority of GaitFormer and indicate that GaitFormer has great potential for learning discriminative representations with more fine-grained temporal dependencies among cross-view walking silhouettes.

4.3.2 Results on CASIA-B and GREW

The results on CASIA-B dataset and GREW dataset are shown in Table 3 and Table 2 respectively. GaitFormer surpasses other SOTA methods on both the small-scale CASIA-B dataset and large-scale GREW dataset. It is worth noting that the number of samples of CASIA-B is too limited and easily overfitted with the transformer framework, the original GaitFormer bears an observable performance drop. As a simple remedy, we utilize the model pre-trained on OU-MVLP to finetune on the CASIA-B dataset, which enables the GaitFormer with a wide leading margin. In the challenging setup of GREW, GaitFormer

Methods	FLOPs	Params	Accuracy
GaitSet [3]	12.91G	6.3M	87.1
GaitPart [13]	7.93G	4.8M	88.7
GLN [18]	73.55G	8.5M	89.2
GaitGL [29]	58.64G	95.6M	89.7
3DLocal [20]	11.17G	4.3M	90.9
GaitFormer	9.62G	51.0M	91.6

Table 5: The analysis of model complexity on OU-MVLP. The number of average floating-point operations (FLOPs) and the parameter number (Params) are reported.

Layer Number	n = 4	n = 5	n = 6	n = 7
Rank-1 Accuracy	90.85	90.71	91.6	91.26

Table 6: The ablation study for layer number in TAM.

still achieves promising results, rank-1 accuracy reaches 65.53%, which is significantly higher than previous methods. The results validate the effectiveness of our framework, showing that GaitFormer is robust even in the presence of wild and unconstrained settings.

4.4. Ablation Study

Several ablation studies with various settings will be conducted on the OU-MVLP dataset to verify the effectiveness of each component in GaitFormer, including the components ablation, T_d in AFPE, layer numbers in TAM, and the results of other baselines plugged with TPA.

GaitFormer Components Ablation. To explore the contribution of the baseline and proposed modules, we conduct

Ablation	Temporal Operation	AFPE	TAM	OU-MVLP	GREW
GaitFormer	Transformer	✓	✓	91.60	65.53
GaitFormer w/o TPA	Max Pooling	✗	✗	87.20	50.94
GaitFormer with decoder	vanilla Transformer	✗	✗	90.51	62.52
GaitFormer w/o AFPE	Transformer	✗	✓	91.24	63.74
GaitFormer w/o TAM	Transformer	✓	✗	91.20	63.50

Table 7: Ablation study of GaitFormer on OU-MVLP and GREW dataset. The number of transformer blocks is set as 6 in experiments.

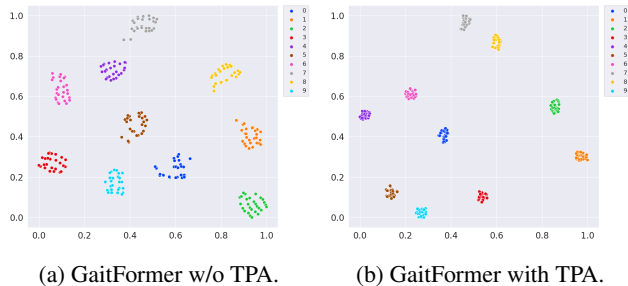


Figure 6: (a) and (b) show the t-SNE visualization examples of GaitFormer w/o TPA and GaitFormer on OU-MVLP test dataset. We visualize 10 identities and each point represents a sample and each color defines a class.

ablation experiments on the OU-MVLP dataset to exploit the role of different parts. The experimental results are shown in Table 7. We can observe that GaitFormer with little temporal pooling achieves poor performance, while the absence of AFPE or TAM brings about severe performance drop, which signifies the importance of these components for producing better representations for gait recognition. Figure 6 consistently demonstrates the effectiveness of TPA from the perspective of feature visualization.

Results of other baselines plugged with TPA To verify that our proposed TPA module is an easy-to-use plug-in technique, we replace the temporal aggregation component of other sequence-based baselines with the TPA module. The results of these baselines plugged with the TPA module are shown in Table 4. As we can see, the performance of these methods was further improved when integrated with TPA. This demonstrates that TPA consistently delivers excellent performance with different backbones, proving its portability and robustness.

GaitFormer taps into periodic dependencies To further prove that GaitFormer indeed extracts potential periodic dependencies, we visualize the feature similarity between each frame in a single gait sequence. As shown in Figure 4, the similarity between the features generated by the base-

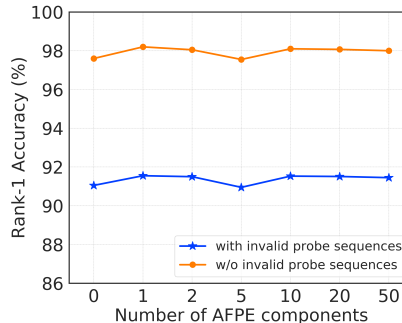


Figure 7: The average rank-1 accuracies with different numbers of AFPE components on the OU-MVLP dataset.

line method GaitPart and GaitGL does not have an obvious periodic trend, while the feature similarity of GaitFormer exhibit a periodic distribution. This demonstrates that the TPA module can indeed inject periodic prior to facilitate training. Furthermore, in order to reveal the learned periodicity of GaitFormer more intuitively, we display the original gait silhouettes along with the similarity in Figure 5. Such results further demonstrate the effectiveness of GaitFormer.

Impact of the layer number in TAM TAM is incorporated to better decompose the temporal signals. Table 6 shows results of TAM with different numbers of layers. The experiments are conducted on the OU-MVLP dataset. It can be observed that TAM with 6 layers achieves better performance compared with other variants while deeper TAM will bring high computational costs.

Impact of T_d in AFPE The component number of the AFPE is empirically set to 1 through our experiments. Here we provide the results on the OU-MVLP dataset in Figure 7 with different component numbers T_d in AFPE. GaitFormer achieves the best performance when T_d is set to 1. This is consistent with the results we obtained by visualizing the OU-MVLP dataset, where the period of gait silhouettes is about 30 frames. When T_d is too large, the transform periodic transformer tends to overfit the complex AFPE.

5. Conclusion

In this work, we propose a plug-and-play strategy named Temporal Periodic Alignment (TPA) for gait recognition to make capital of the periodic inductive bias. Specifically, TPA encapsulates two key components, Adaptive Fourier-transform Position Encoding (AFPE) which injects the period prior, and Temporal Aggregation Module (TAM) which explores fine-grained temporal dependencies. We further build a simple yet strong baseline GaitFormer on the basis of TPA. Extensive experiments are conducted on several datasets to verify the effectiveness of these components.

A. More Details of Implementation

A.1. Framework of TAM

Temporal Aggregation Module (TAM) is composed of Multi-Head Cross-Attention (MHCA) sub-layer and a position-wise feed-forward network (FFN), where the period-aware embeddings and tokens are directly sent into MHCA sub-layer to extract temporal information. The output feature computes temporal triplet loss as a temporal representation. At the same time, it is also sent into a fusion module to generate global features as classification representations. For the understanding of decomposition, inspired by time-series regression, input series are separated into trend-cyclical and seasonal parts, which reflect long-term progression and seasonality respectively. For gait recognition, the seasonal parts reflect the periodic template of the walking pattern, while the trend-cyclical parts mostly display shape and appearance.

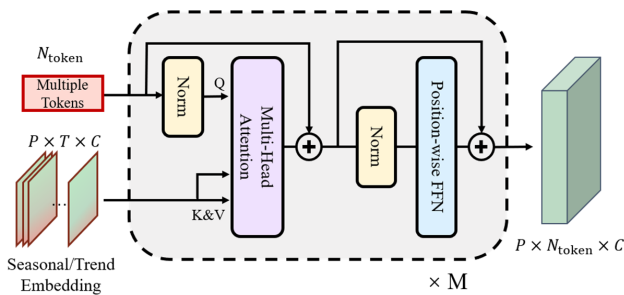


Figure 8: Framework of the TAM module.

A.2. Details of training objectives

As mentioned, we replace the vanilla CE loss with the ArcFace loss [8] to produce a larger margin. Marginal losses like ArcFace are widely adopted in face recognition and re-identification. The ArcFace loss is an improved version of cross-entropy loss, which introduces angular distance to constrain the distance between features of different categories. Thanks to the scale and angular margin, ArcFace loss achieves better generalization performance in face

Ablation	OU-MVLP
GaitFormer	91.60
GaitFormer with Cross Entropy	91.20
GaitFormer with vanilla PE	90.51

Table 8: Ablation study of GaitFormer on OU-MVLP dataset. The number of transformer blocks is set as 6 in experiments.

recognition and person re-identification tasks. Empirically We find that ArcFace brings faster and better convergence of experiments. The ArcFace loss can be formatted as:

$$L_{cls} = -\frac{1}{N} \sum_{i=1}^N \log \frac{e^{s \cdot (\cos(\theta_{y_i} + m))}}{e^{s \cdot (\cos(\theta_{y_i} + m))} + \sum_{j=1, j \neq y_i}^n e^{s \cdot \cos(\theta_j)}} \quad (9)$$

where N and n indicate batch size and class number, s and m are the scale and margin mentioned above, y_i means the class index of the i th instance, θ_j is the angle between the project layer weight and the i th feature. We set $s = 32$ and $m = 0.3$ in our experiments.

B. Additional Experiment Results

In this section, we will give some additional detailed experimental results and related analyses. The results of other baselines are copied from their original papers.

B.1. Visualization of AFPE feature

The AFPE is introduced to encode a series of discrete time and extend the original signals into the positional-aware embeddings in an adaptive manner. Hence it is important to observe the final results generated by AFPE. The shape of the final AFPE is $1 \times T \times C$, where T is the total frames of the sequence on the temporal dimension and C is the same as the input feature dimensions. The first row in Figure 9 shows 10 randomly selected base sequences and the second row shows the trend of the average AFPE result, which is the final AFPE added with embeddings. Such visualization is consistent with the assumption that the gait sequence is a composite of multiple similar periods.

B.2. Additional results for GaitFormer

Additional results under different Views on CASIA-B dataset We provide detailed results under different probe views on the CASIA-B dataset in Table 9. There are 11 views ($0^\circ, 18^\circ, \dots, 180^\circ$) under NM, BG and CL variants. It is worth noting that the number of samples of CASIA-B is too limited and easily overfitting with the transformer framework, so we utilize the model pre-trained on OU-MVLP to finetune on CASIA-B dataset. Here methods with '+' denote two-stage training, warm-up on OUVMLP and

Probe	Method	Probe View											Mean
		0°	18°	36°	54°	72°	90°	108°	126°	144°	162°	180°	
NM	GaitSet	90.8	97.9	99.4	96.9	93.6	91.7	95.0	97.8	98.9	96.8	85.8	95.0
	GaitPart	94.1	98.6	99.3	98.5	94.0	92.3	95.9	98.4	99.2	97.8	90.4	96.2
	ReverseMask	96.5	98.4	99.2	98.0	97.1	95.5	97.4	99.2	99.3	99.1	95.0	97.7
	GaitGL	96.0	98.3	99.0	97.9	96.9	95.4	97.0	98.9	99.3	98.8	94.0	97.4
	3DLocal	96.0	99.0	99.5	98.9	97.1	94.2	96.3	99.0	98.8	98.5	95.2	97.5
	GaitSet+	94.2	98.2	99.7	97.5	95.6	94.9	95.8	97.7	98.1	97.5	93.3	96.9
	GaitGL+	96.3	98.5	99.2	98.3	98.4	97.7	98.8	99.8	99.7	99.4	97.1	98.5
	GaitFormer+	97.0	100.0	100.0	99.7	98.8	97.8	98.0	99.7	99.7	99.7	97.7	98.9
BG	GaitSet	83.8	91.2	91.8	88.8	83.3	81.0	84.1	90.0	92.2	94.4	79.0	87.2
	GaitPart	89.1	94.8	96.7	95.1	88.3	84.9	89.0	93.5	96.1	93.8	85.8	91.5
	ReverseMask	93.7	97.0	97.3	95.8	94.9	91.4	93.5	97.3	98.3	97.3	92.4	95.3
	GaitGL	92.6	96.6	96.8	95.5	93.5	89.3	92.2	96.5	98.2	96.9	91.5	94.5
	3DLocal	92.9	95.9	97.8	96.2	93.0	87.8	92.7	96.3	97.9	98.0	88.5	94.3
	GaitSet+	89.6	94.9	95.2	93.3	89.9	86.7	90.8	94.5	97.2	97.7	87.3	92.6
	GaitGL+	94.0	96.7	97.0	96.2	94.5	91.0	93.7	96.8	98.6	97.7	92.6	95.3
	GaitFormer+	92.2	97.7	97.1	95.8	94.1	87.6	93.1	96.5	98.1	97.5	92.3	94.7
CL	GaitSet	61.4	75.4	80.7	77.3	72.1	70.1	71.5	73.5	73.5	68.4	50.0	70.4
	GaitPart	70.7	85.5	86.9	83.3	77.1	72.5	76.9	82.2	83.8	80.2	66.5	78.7
	ReverseMask	78.9	91.5	93.1	91.1	85.6	81.0	85.2	89.0	90.9	87.3	72.9	86.0
	GaitGL	76.6	90.0	90.3	87.1	84.5	79.0	84.1	87.0	87.3	84.4	69.5	83.6
	3DLocal	78.2	90.2	92.0	87.1	83.0	76.8	83.1	86.6	86.8	84.1	70.9	83.7
	GaitSet+	72.0	86.3	89.7	87.6	80.2	79.1	80.9	82.2	86.5	78.7	69.6	81.7
	GaitGL+	77.0	93.2	92.9	90.5	83.8	81.3	85.0	89.7	90.1	86.0	73.9	85.8
	GaitFormer+	77.3	88.8	92.9	93.1	88.6	82.1	85.2	91.0	92.7	90.5	78.2	87.3

Table 9: Rank-1 accuracy (%) of the compared method on CASIA-B under different probe views, excluding identical-view cases with the setting of large-scale training (LT, i.e., 74 subjects for training),.

Methods	TPA	FLOPs	Params	Accuracy
GaitPart [13]	✗	7.93G	4.8M	88.7
	✓	8.41G	9.8M	89.4
GaitGL [29]	✗	58.64G	95.6M	89.7
	✓	59.44G	100.6M	90.4
MetaGait* [11]	✗	58.64G	95.8M	89.1
	✓	59.19G	99.1M	89.6

Table 10: The FLOPs and parameters before and after we replace the Temporal Aggregator with our TPA strategy. It can be observed that our TPA strategy brings perceptible improvement, with small increase in calculation and parameters amount. MetaGait* represents our implementation of MetaGait, which is lower than the result in the origin paper.

continue the second stage of training and testing on CASIA-B dataset.

Additional ablation of GaitFormer Components we conduct more ablation experiments on the OU-MVLP dataset to explore the contribution of the modules. The experimental results are shown in Table 8.

We can observe that GaitFormer with vanilla CE bears slight performance degradation. Moreover, the vanilla po-

sition encoding (PE) regards each element as unique and our proposed AFPE force the network to exploit periodic prior. Table 8 compares the performance with AFPE and vanilla PE and the proposed AFPE is shown to excel, which demonstrates the effectiveness of our proposed AFPE.

Advantages of GaitFormer Compared with temporal normalization [28] and phase synchronization [34]. GaitFormer resorts to attention mechanisms to explicitly explore the temporal dependencies between different frames in the walking sequence. Such paradigms of temporal fusion are more intuitive and effective, which is displayed in our visualizations.

References

- [1] Weizhi An, Shiqi Yu, Yasushi Makihara, Xinhui Wu, Chi Xu, Yang Yu, Rijun Liao, and Yasushi Yagi. Performance evaluation of model-based gait on multi-view very large population database with pose sequences. *IEEE transactions on biometrics, behavior, and identity science*, 2(4):421–430, 2020.
- [2] Tianrui Chai, Annan Li, Shaoxiong Zhang, Zilong Li, and Yunhong Wang. Lagrange motion analysis and view embeddings for improved gait recognition. In *CVPR*, pages 20217–20226. IEEE, 2022.
- [3] Hanqing Chao, Yiwei He, Junping Zhang, and Jianfeng Feng. Gaitset: Regarding gait as a set for cross-view gait

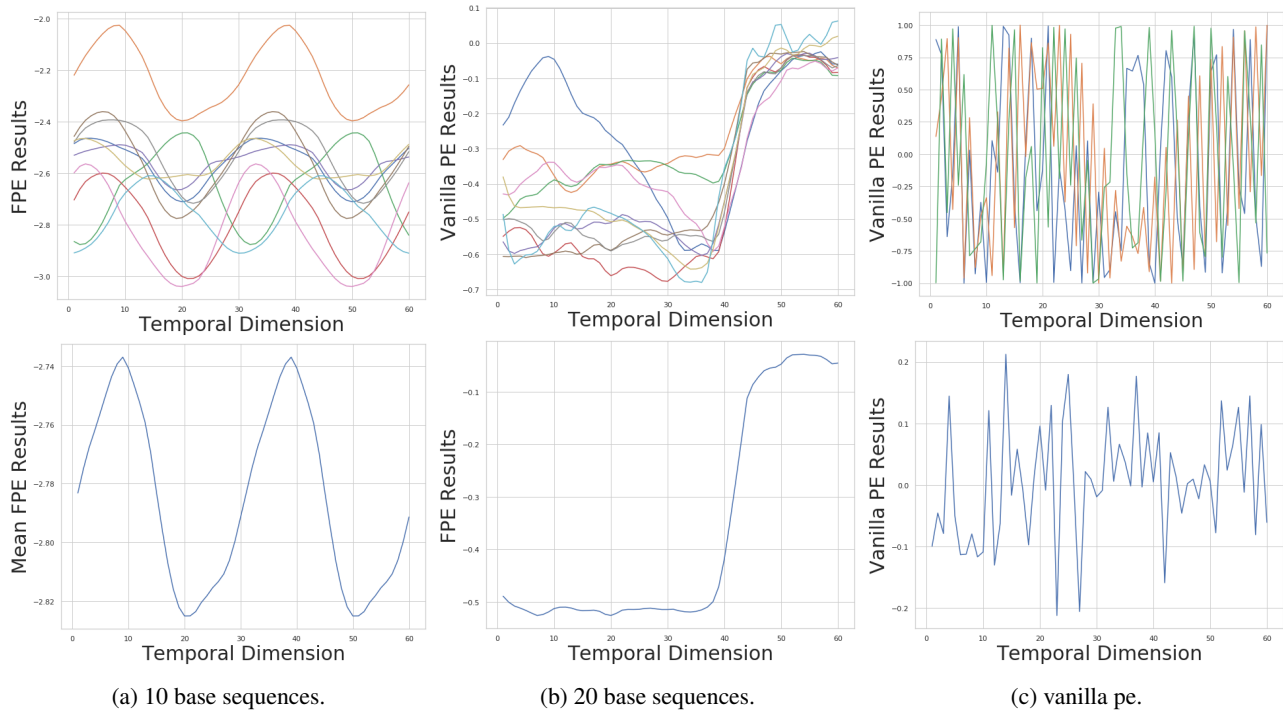


Figure 9: AFPE and average amplitude of different experimental configurations of base sequences. If the number of base sequences is greater than 10, then 10 samples are randomly sampled from all sequences.

- recognition. In *The Thirty-Third AAAI Conference on Artificial Intelligence, AAAI 2019, The Thirty-First Innovative Applications of Artificial Intelligence Conference, IAAI 2019, The Ninth AAAI Symposium on Educational Advances in Artificial Intelligence, EAAI 2019, Honolulu, Hawaii, USA, January 27 - February 1, 2019*, pages 8126–8133. AAAI Press, 2019.
- [4] Xiangxiang Chu, Zhi Tian, Bo Zhang, Xinlong Wang, Xiaolin Wei, Huaxia Xia, and Chunhua Shen. Conditional positional encodings for vision transformers. *arXiv preprint arXiv:2102.10882*, 2021.
- [5] Robert B Cleveland, William S Cleveland, Jean E McRae, and Irma Terpenning. Stl: A seasonal-trend decomposition. *J. Off. Stat.*, 6(1):3–73, 1990.
- [6] Patrick Connor and Arun Ross. Biometric recognition by gait: A survey of modalities and features. *Computer Vision and Image Understanding*, 167:1–27, 2018.
- [7] David Cunado, Mark S Nixon, and John N Carter. Using gait as a biometric, via phase-weighted magnitude spectra. In *Audio-and Video-based Biometric Person Authentication: First International Conference, AVBPA'97 Crans-Montana, Switzerland, March 12–14, 1997 Proceedings 1*, pages 93–102. Springer, 1997.
- [8] Jiankang Deng, Jia Guo, Niannan Xue, and Stefanos Zafeiriou. Arcface: Additive angular margin loss for deep face recognition. In *Proceedings of the IEEE/CVF conference on computer vision and pattern recognition*, pages 4690–4699, 2019.
- [9] Alexey Dosovitskiy, Lucas Beyer, Alexander Kolesnikov, Dirk Weissenborn, Xiaohua Zhai, Thomas Unterthiner, Mostafa Dehghani, Matthias Minderer, Georg Heigold, Sylvain Gelly, et al. An image is worth 16x16 words: Transformers for image recognition at scale. *arXiv preprint arXiv:2010.11929*, 2020.
- [10] Huanzhang Dou, Pengyi Zhang, Wei Su, Yunlong Yu, and Xi Li. Metagait: Learning to learn an omni sample adaptive representation for gait recognition. In *ECCV*, volume 13665 of *Lecture Notes in Computer Science*, pages 357–374. Springer, 2022.
- [11] Huanzhang Dou, Pengyi Zhang, Wei Su, Yunlong Yu, and Xi Li. Metagait: Learning to learn an omni sample adaptive representation for gait recognition. In *Computer Vision—ECCV 2022: 17th European Conference, Tel Aviv, Israel, October 23–27, 2022, Proceedings, Part V*, pages 357–374. Springer, 2022.
- [12] Chao Fan, Junhao Liang, Chuanfu Shen, Saihui Hou, Yongzhen Huang, and Shiqi Yu. Opengait: Revisiting gait recognition towards better practicality. In *Proceedings of the IEEE/CVF Conference on Computer Vision and Pattern Recognition (CVPR)*, pages 9707–9716, June 2023.
- [13] Chao Fan, Yunjie Peng, Chunshui Cao, Xu Liu, Saihui Hou, Jiannan Chi, Yongzhen Huang, Qing Li, and Zhiqiang He. Gaitpart: Temporal part-based model for gait recognition. In *2020 IEEE/CVF Conference on Computer Vision and Pattern Recognition, CVPR 2020, Seattle, WA, USA, June 13–19, 2020*, pages 14213–14221. Computer Vision Foundation / IEEE, 2020.

- [14] Yang Feng, Yuncheng Li, and Jiebo Luo. Learning effective gait features using LSTM. In *23rd International Conference on Pattern Recognition, ICPR 2016, Cancún, Mexico, December 4-8, 2016*, pages 325–330. IEEE, 2016.
- [15] Ju Han and Bir Bhanu. Individual recognition using gait energy image. *IEEE Trans. Pattern Anal. Mach. Intell.*, 28(2):316–322, 2006.
- [16] Sepp Hochreiter and Jürgen Schmidhuber. Long short-term memory. *Neural computation*, 9(8):1735–1780, 1997.
- [17] Elad Hoffer and Nir Ailon. Deep metric learning using triplet network. In *Similarity-Based Pattern Recognition: Third International Workshop, SIMBAD 2015, Copenhagen, Denmark, October 12-14, 2015. Proceedings 3*, pages 84–92. Springer, 2015.
- [18] Saihui Hou, Chunshui Cao, Xu Liu, and Yongzhen Huang. Gait lateral network: Learning discriminative and compact representations for gait recognition. In Andrea Vedaldi, Horst Bischof, Thomas Brox, and Jan-Michael Frahm, editors, *Computer Vision - ECCV 2020 - 16th European Conference, Glasgow, UK, August 23-28, 2020, Proceedings, Part IX*, volume 12354 of *Lecture Notes in Computer Science*, pages 382–398. Springer, 2020.
- [19] Xiaohu Huang, Duowang Zhu, Hao Wang, Xinggong Wang, Bo Yang, Botao He, Wenyu Liu, and Bin Feng. Context-sensitive temporal feature learning for gait recognition. In *Proceedings of the IEEE/CVF International Conference on Computer Vision*, pages 12909–12918, 2021.
- [20] Zhen Huang, Dixiu Xue, Xu Shen, Xinmei Tian, Houqiang Li, Jianqiang Huang, and Xian-Sheng Hua. 3d local convolutional neural networks for gait recognition. In *Proceedings of the IEEE/CVF International Conference on Computer Vision*, pages 14920–14929, 2021.
- [21] Sergey Ioffe and Christian Szegedy. Batch normalization: Accelerating deep network training by reducing internal covariate shift. In *International conference on machine learning*, pages 448–456. PMLR, 2015.
- [22] Guodong Li, Lijun Guo, Rong Zhang, Jiangbo Qian, and Shangce Gao. Transgait: Multimodal-based gait recognition with set transformer. *Applied Intelligence*, pages 1–13, 04 2022.
- [23] Guodong Li, Lijun Guo, Rong Zhang, Jiangbo Qian, and Shangce Gao. Transgait: Multimodal-based gait recognition with set transformer. *Applied Intelligence*, pages 1–13, 2022.
- [24] Xiang Li, Yasushi Makihara, Chi Xu, and Yasushi Yagi. Multi-view large population gait database with human meshes and its performance evaluation. *IEEE Transactions on Biometrics, Behavior, and Identity Science*, 4(2):234–248, 2022.
- [25] Xiang Li, Yasushi Makihara, Chi Xu, Yasushi Yagi, Shiqi Yu, and Mingwu Ren. End-to-end model-based gait recognition. In *ACCV*, volume 12624, pages 3–20. Springer, 2020.
- [26] Junhao Liang, Chao Fan, Saihui Hou, Chuanfu Shen, Yongzhen Huang, and Shiqi Yu. Gaitedge: Beyond plain end-to-end gait recognition for better practicality. In *ECCV*, volume 13665, pages 375–390. Springer, 2022.
- [27] Rijun Liao, Chunshui Cao, Edel B Garcia, Shiqi Yu, and Yongzhen Huang. Pose-based temporal-spatial network (ptsn) for gait recognition with carrying and clothing variations. In *CCBR*, 2017.
- [28] Rijun Liao, Shiqi Yu, Weizhi An, and Yongzhen Huang. A model-based gait recognition method with body pose and human prior knowledge. *Pattern Recognit.*, 98, 2020.
- [29] Beibei Lin, Shunli Zhang, and Xin Yu. Gait recognition via effective global-local feature representation and local temporal aggregation. In *2021 IEEE/CVF International Conference on Computer Vision, ICCV 2021, Montreal, QC, Canada, October 10-17, 2021*, pages 14628–14636. IEEE, 2021.
- [30] Yingfei Liu, Tiancai Wang, Xiangyu Zhang, and Jian Sun. Petr: Position embedding transformation for multi-view 3d object detection. *arXiv preprint arXiv:2203.05625*, 2022.
- [31] Ze Liu, Yutong Lin, Yue Cao, Han Hu, Yixuan Wei, Zheng Zhang, Stephen Lin, and Baining Guo. Swin transformer: Hierarchical vision transformer using shifted windows. In *Proceedings of the IEEE/CVF International Conference on Computer Vision*, pages 10012–10022, 2021.
- [32] Ze Liu, Jia Ning, Yue Cao, Yixuan Wei, Zheng Zhang, Stephen Lin, and Han Hu. Video swin transformer. In *Proceedings of the IEEE/CVF Conference on Computer Vision and Pattern Recognition*, pages 3202–3211, 2022.
- [33] Ilya Loshchilov and Frank Hutter. Decoupled weight decay regularization. *arXiv preprint arXiv:1711.05101*, 2017.
- [34] Atsushi Mori, Yasushi Makihara, and Yasushi Yagi. Gait recognition using period-based phase synchronization for low frame-rate videos. In *2010 20th International Conference on Pattern Recognition*, pages 2194–2197, 2010.
- [35] Trong-Nguyen Nguyen, Huu-Hung Huynh, and Jean Meunier. Skeleton-based gait index estimation with lstms. In *17th IEEE/ACIS International Conference on Computer and Information Science, ICIS 2018, Singapore, Singapore, June 6-8, 2018*, pages 468–473. IEEE Computer Society, 2018.
- [36] Adam Paszke, Sam Gross, Francisco Massa, Adam Lerer, James Bradbury, Gregory Chanan, Trevor Killeen, Zeming Lin, Natalia Gimelshein, Luca Antiga, et al. Pytorch: An imperative style, high-performance deep learning library. *Advances in neural information processing systems*, 32, 2019.
- [37] Alireza Sepas-Moghaddam and Ali Etemad. Deep gait recognition: A survey. *IEEE Transactions on Pattern Analysis and Machine Intelligence*, 2022.
- [38] Chuanfu Shen, Beibei Lin, Shunli Zhang, George Q Huang, Shiqi Yu, and Xin Yu. Gait recognition with mask-based regularization. *arXiv preprint arXiv:2203.04038*, 2022.
- [39] Chuanfu Shen, Beibei Lin, Shunli Zhang, George Q. Huang, Shiqi Yu, and Xin Yu. Gait recognition with mask-based regularization. *CoRR*, abs/2203.04038, 2022.
- [40] Chuanfu Shen, Shiqi Yu, Jilong Wang, George Q Huang, and Liang Wang. A comprehensive survey on deep gait recognition: Algorithms, datasets and challenges. *arXiv preprint arXiv:2206.13732*, 2022.
- [41] Kohei Shiraga, Yasushi Makihara, Daigo Muramatsu, Tomio Echigo, and Yasushi Yagi. Geinet: View-invariant gait recognition using a convolutional neural network. In *International Conference on Biometrics, ICB 2016, Halmstad, Sweden, June 13-16, 2016*, pages 1–8. IEEE, 2016.

- [42] Kohei Shiraga, Yasushi Makihara, Daigo Muramatsu, Tomio Echigo, and Yasushi Yagi. Geinet: View-invariant gait recognition using a convolutional neural network. In *2016 international conference on biometrics (ICB)*, pages 1–8. IEEE, 2016.
- [43] Noriko Takemura, Yasushi Makihara, Daigo Muramatsu, Tomio Echigo, and Yasushi Yagi. Multi-view large population gait dataset and its performance evaluation for cross-view gait recognition. *IPSJ Trans. Comput. Vis. Appl.*, 10:4, 2018.
- [44] Noriko Takemura, Yasushi Makihara, Daigo Muramatsu, Tomio Echigo, and Yasushi Yagi. On input/output architectures for convolutional neural network-based cross-view gait recognition. *IEEE Transactions on Circuits and Systems for Video Technology*, 29(9):2708–2719, 2019.
- [45] Daoliang Tan, Kaiqi Huang, Shiqi Yu, and Tieniu Tan. Efficient night gait recognition based on template matching. In *18th International Conference on Pattern Recognition (ICPR 2006), 20-24 August 2006, Hong Kong, China*, pages 1000–1003. IEEE Computer Society, 2006.
- [46] Ashish Vaswani, Noam Shazeer, Niki Parmar, Jakob Uszkoreit, Llion Jones, Aidan N Gomez, Łukasz Kaiser, and Illia Polosukhin. Attention is all you need. *Advances in neural information processing systems*, 30, 2017.
- [47] Limin Wang, Yuanjun Xiong, Zhe Wang, Yu Qiao, Dahua Lin, Xiaoou Tang, and Luc Van Gool. Temporal segment networks for action recognition in videos. *IEEE transactions on pattern analysis and machine intelligence*, 41(11):2740–2755, 2018.
- [48] Zifeng Wu, Yongzhen Huang, Liang Wang, Xiaogang Wang, and Tieniu Tan. A comprehensive study on cross-view gait based human identification with deep cnns. *IEEE transactions on pattern analysis and machine intelligence*, 39(2):209–226, 2016.
- [49] Zifeng Wu, Yongzhen Huang, Liang Wang, Xiaogang Wang, and Tieniu Tan. A comprehensive study on cross-view gait based human identification with deep cnns. *IEEE Trans. Pattern Anal. Mach. Intell.*, 39(2):209–226, 2017.
- [50] Weiwei Xing, Ying Li, and Shunli Zhang. View-invariant gait recognition method by three-dimensional convolutional neural network. *Journal of Electronic Imaging*, 27:1, 01 2018.
- [51] Shiqi Yu, Daoliang Tan, and Tieniu Tan. A framework for evaluating the effect of view angle, clothing and carrying condition on gait recognition. In *ICPR*, volume 4, pages 441–444. IEEE, 2006.
- [52] Cheng Zhang, Wu Liu, Huadong Ma, and Huiyuan Fu. Siamese neural network based gait recognition for human identification. In *2016 IEEE International Conference on Acoustics, Speech and Signal Processing, ICASSP 2016, Shanghai, China, March 20-25, 2016*, pages 2832–2836. IEEE, 2016.
- [53] Zheng Zhu, Xianda Guo, Tian Yang, Junjie Huang, Jiankang Deng, Guan Huang, Dalong Du, Jiwen Lu, and Jie Zhou. Gait recognition in the wild: A benchmark. In *Proceedings of the IEEE/CVF international conference on computer vision*, pages 14789–14799, 2021.